General Disclaimer

One or more of the Following Statements may affect this Document

- This document has been reproduced from the best copy furnished by the organizational source. It is being released in the interest of making available as much information as possible.

- This document may contain data, which exceeds the sheet parameters. It was furnished in this condition by the organizational source and is the best copy available.

- This document may contain tone-on-tone or color graphs, charts and/or pictures, which have been reproduced in black and white.

- This document is paginated as submitted by the original source.

- Portions of this document are not fully legible due to the historical nature of some of the material. However, it is the best reproduction available from the original submission.

Produced by the NASA Center for Aerospace Information (CASI)

FINAL REPORT

GRANT NAGW-652

"Trapped Particle Absorption by the Ring of Jupiter"

NOV 1985
RECEIVED
NASA STI FACILITY
ACCESS DEPT.

Prepared by

Walker Fillius, Principal Investigator

Center for Astrophysics and Space Sciences

University of California, San Diego

La Jolla, California, 92093

for the period 9/1/84 to 8/31/85

INTRODUCTION

The ring systems of Jupiter and Saturn, and their interaction with the magnetosphere, are the focus of our work on this grant. We still see opportunities to improve our understanding of the sweeping effect of orbiting material on trapped radiation, and to use this process to gain insight on both the trapped radiation and the target material. Within the cosmogony of Hannes Alfven, this mechanism is also the key to understanding the formation of many of the features of the Saturnian rings. A better understanding of the sweeping effect would help to this process as well.

PROGRESS

Jupiter's Synchronous-Altitude "Gossamer" Ring

Recently, Showalter et al [1985] discovered a "gossamer" extension of Jupiter's ring out to almost 3 RJ, with a slight but definite peak at synchronous altitude. We were able to contribute to an explanation for this feature [Mendis et al, 1985]. Mendis, Hill, and Northrop had already discovered that charged dust grains undergo a radial "gyro-drift," associated with a variation of the charge on the grain during the phases of the gyro motion. Because the phase of the charge variation is determined by the difference between the Keplerian and corotating velocities, synchronous altitude is a special location where the drift vanishes. From other positions, the drift is directed toward synchronous altitude. This effect was apparently unknown to Showalter before his discovery, although it would be fair to say that Mendis's associates "predicted" a ring at synchronous altitude. We believe the "gyro-drift" is the best explanation for this feature. Incidentally, this mechanism also confirms the existence of charge on the dust grains. A copy of the Mendis et al paper is appended to this report.

Showalter, M. R., J. A. Burns, J. N. Cuzzi, and J. B. Pollack, "The Discovery of a Tenuous Jovian Ring," Nature, 1985.

Mendis, D. A., J. R. Hill, T. N. Northrop, and W. Fillius, "A Note on Jupiter's 'Gossamer' Ring," submitted to Nature, 1985.

High Energy Protons in the Vicinity of Saturn's G Ring

During this past year we completed a joint project with Ted Northrop at GSFC, Bernie Blake at Aerospace Corporation, and Steve Margolis at St. Louis University, which has now gotten two papers into press. This project started with the proposition of Fillius et al [1980] and Fillius and McIlwain [1980] that the high energy protons in Saturn's inner radiation belts originated as the decay products of a neutron albedo created by cosmic rays interacting with the rings. Blake and Margolis postulated that there might be a belt of very high energy electrons as well, produced by cosmic ray interactions with the moons Mimas, Janus, and Epimetheus. There had been a suggestion of such an electron belt in the UCSD data from the Pioneer 11 encounter, but there was a problem with distinguishing protons from electrons in the data. Northrop developed an elegant technique for separating the different species by using the angular distributions, and we applied this technique to the data. We were able to establish the intensities of >500 MeV protons, >5 MeV electons, their radial profiles, and, to first order, their angular distributions. The result was disappointing to Blake and Margolis, as the radial profile of the electrons conflicted with their expectations. Most likely the source is not moon albedo. However, the project does improve our knowledge of the trapped radiation levels and give us a better understanding of the interactions between orbiting material and the trapped radiation. A copy of the Northrop-Fillius paper is appended to this report.

Northrop, Theodore G., and Walker Fillius, "Electrons and Cosmic Ray Produced Protons in Saturn's Inner Magnetosphere," in press, J. Geophys. Res., 1985.

Northrop, Theodore G., "Relationships Among the Harmonic Coefficients of Scan Plane Anisotropies," in press, J. Geophys. Res., 1985.

Fillius, W., and C. McIlwain, "Very Energetic Protons in Saturn's Radiation Belt," J. Geophys. Res., 85, 5803-5811, Nov. 1, 1980.

Absorption of Trapped Particles by Orbiting Material

We have studied the expected effects of absorbing material on the trapped radiation to obtain the loss rate as a function of ring properties. For the case of azimuthal symmetry and random probability of impact, we have an analytical expression valid for all sizes of absorbers and all particle gyroradii and pitch angles. For a known absorber, we can then calculate the absorption probability. We are particularly concerned with the inverse problem: given the loss rate, deduce the poperties of the ring.

Applying the loss probability to the particle diffusion equation rounds out the theoretical end of the ring absorption problem. There are two approaches, one quick and dirty and hard to justify, and the other slow, dirty, and easy to justify. We wrote a paper using the first approach [Fillius, W., M. F. Thomsen, J. A. Van Allen, W.-H. Ip, M. Acuna, and N. F. Ness, "Trapped Radiation Absorption at the Ring of Jupiter"], but held up publication because of the critical nature of the results. We want to do a more thorough analysis, developing both approaches in a way that illuminates the relationship between their results, before we announce our conclusions.

In collaboration with Bernie Blake at Aerospace Corporation, we have used our experience with the satellite sweeping problem to comment on a search for a satellite imbedded in Saturn's G ring [Blake, J. B., and W. Fillius, "On the Maximum Size of a Satellite at Saturn's G-Ring," paper read at the 1984 meeting of the Division of Planetary Sciences of the American Astronimical Society]. Our conclusion was that any satellite would be too small to detect from earth. The abstract of this paper is appended to this report.

Scientific Value of High Energy Particle Measurements on a Jupiter Polar Orbiter

A the request of George Siscoe and Tom Krimigis, we contributed a section on energetic charged particle measurements to a report on prospects for a future Jupiter Orbiter Mission. There is a lot of good science that can

be done from the any of the proposed orbits, and the mission i .ds very interesting. The section on high energy particle measurements is appended to this report.

.

POSSIBILITIES FOR FUTURE RESEARCH

The spatial profile of the absorbing ring material is also immersed in the trapped radiation data as a deconvolution of the absorption profile with the magnetic field line spread function. Although we have line spread functions, we have found that the location of the absorbers can be inferred accurately only by doing a numerical integration of the particle diffusion equation, using a model for the particle latitude distribution. Such models have been unsatisfactory to date, but we believe that angular distribution data will give us enough of a handle to make this procedure tractable. The result matters in the case of the Jupiter ring, because neither the visible ring of micron-sized particles nor the shepherding moons appear to be responsible for all of the trapped radiation absorption. Thus we are inferring the location of an invisible component, which is probably also the parent material, or "mooms," for the dust ring.

We would also like to solve the problem encountered with the Jovian electrons, where there are synchrotron losses in addition to the ring absorption. This will require a numerical approach, which we are developing anyway. Our hypothesis, which we hope to substantiate, is that this accounts for an apparent difference between the amount of ring material encountered by the electrons and by the protons.

Finally, we note that the principles and techniques developed here for the Jovian ring are applicable to Saturn and Uranus as well. Going further, Hannes Alfven explicitly cites the spatial profile of Saturn's A, B, and C rings as evidence that these sweeping mechanisms took place four billion years ago during the formation of the solar system. The work is difficult, but worthwhile.

THE SCIENTIFIC VALUE OF HIGH ENERGY PARTICLE
MEASUREMENTS ON A JUPITER POLAR ORBITER

HIGH ENERGY PARTICLES

The inner magnetosphere of Jupiter contains the highest energy, locally-accelerated particles in the solar system, and the greatest variety of energetic particle source, acceleration, transport, and loss mechanisms within reach of in situ measurements. Io interacts strongly with the energetic particles, and leaves its signature on the population in many ways. Including the Io-related processes, many of phenomena can only be studied from a close-in Jovian orbit. Other processes, which occur at earth and/or other planets, must also be studied here in order to develop a general theory of magnetospheres which can be extrapolated to the larger scales of astrophysics.

Sources

Energetic particle sources include the solar wind, the upper planetary atmosphere, and the decay of cosmic ray albedo products, as at earth, plus the unique Io torus. The magnetospheric plasma at Jupiter contains the composition signatures of both the Iogenic source (O, S, K, Na) and the apparent source in the upper ionosphere ($H2+$, $H3+$). Because of these "tracer" elements, it is possible to perform unique studies on acceleration and diffusion processes. For example, one would expect that torus ions would diffuse inward, as well as outward, and that it would be possible to separate clearly at $L < 6$ the contribution to the inner radiation belt of diffusing ions from Io, compared to that from other sources.

Acceleration

Similarly, measurements of the variation of composition and angular distributions with latitude will provide an exceptional tool in studying acceleration processes taking place in the vicinity of Io's flux tube from those operating at high latitude, above Jupiter's auroral region.

The Voyagers found that the equivalent temperatures of particles (> 10 keV) were in the range of ~20-30 keV at large (>20 Rj) L values, and various models have dealt with the heating and acceleration mechanism. If such temperatures persist closer in to the planet, and at high latitudes, our current understanding of the heating mechanism would have to be drastically modified. Therefore it is essential to measure angular distributions of all energetic ions as a function of both latitude and radial distance.

The highest energy particles in the Jovian magnetosphere gain their energy by conserving their first two adiabatic invariants while violating the third and moving inwards. It is well established that this is a diffusive process, which in many ways resembles earth's. However, unlike earth, the diffusion well within Io's orbit is apparently driven by electric fields caused by upper atmospheric tides' crossing magnetic field lines. The

determination of the diffusion coefficient and its radial dependence are important objectives, both for confirming the driving mechanism, and for characterizing the inner radiation belt and its power input. Furthermore, centrifugally driven interchanges and/or large scale convection are thought to occur near and outside Io's orbit. It is also important to explore the possible role of these processes within the inner radiation belts.

The existence of 1-10 MeV electrons in the outer Jovian magnetosphere is paradoxical to this model, because their energy far exceeds that of particles on the diffusion track. Hypotheses have been proposed for acceleration mechanisms, such as recirculation, direct acceleration by parallel electric fields, and magnetic pumping, but there is no consensus, and not enough evidence to support one idea or another. As a spacecraft in an inclined orbit crosses the outer magnetospheric field lines at low altitudes, one can seek evidence here, such as field-aligned particle beams, which would reveal where these particles come from.

The results of such a search could lead to an estimate of the lifetime of these electrons, and this, in turn, could lay to rest the question of whether the outer magnetosphere pulses like a clock, as suggested by the Chicago group, or behaves more stably like a wobbly disk.

Precipitation, Aurora, and the Stably Trapped Limit

In addition to radial diffusion, which accelerates particles, pitch angle diffusion is another mechanism which deserves study. Pitch angle diffusion is caused by the growth of waves which resonate with the trapped particles, perturbing their pitch angles, and the consequences are radio waves, particle precipitation, and aurora. Besides producing provocative visual and UV displays, aurora can inject significant amounts of energy to the upper ionosphere and atmosphere, affecting ionospheric conductivity and atmospheric circulation. We know very little about aurora on Jupiter. Although Galileo will probably see visual displays and add vastly to our knowledge in that arena, the actual particle precipitation is better studied from high latitudes and lower altitudes where the loss cone is large enough to sample. Thus it is likely that Galileo will increase our appetite for direct measurements of the precipitating particles from a polar orbiting spacecraft. These measurements should include complete pitch angle distributions and identification of ion species as well as electrons.

If the flux of a trapped species gets high enough, it becomes unstable to the growth of waves which cause pitch angle scattering and precipitation, which relieve the instability. Both ions and electrons are thought to press this limit between L~5 and 15 RJ. The existence of an electron limit at this position is thought to explain the constancy of the decimetric radiation, because the inwardly diffusing electrons which eventually produce the synchrotron radiation must pass through the equivalent of a regulator before they get to the site of the radiation. These ideas received some support from previous flyby's, but would be greatly enhanced by a more complete survey of electron fluxes in the inner Jovian magnetosphere. The principle of a constant flux valve is a powerful one for simplifying complex dynamical systems, and one which could have applications elsewhere in the cosmos.

Satellite Sweeping Signatures

The isolated satellite sweeping signatures obtained by past flybys have served as valuable diagnostics of diffusive particle behavior, and obtaining multiple orbital crossings would allow refinement of this very fruitful method. With repeated crossings of the appropriate L-shells, satellite sweeping signatures from the ring, Metis, Adrastea, Amalthea, Thebe, Io, Europa, Ganymede, and possibly Callisto can be investigated as a function of longitude. This would allow a better understanding of microsignatures, and their evolution into azimuthally averaged macrosignatures.

Also to be gained from these sweeping signatures would be information about the gross characteristics of the satellites themselves: eg., their magnetic field and conductivity. In prior sweeping studies, satellites have always been considered as non-magnetic, pure insulators, exercising a wholly passive role as absorbers of trapped radiation. However, especially in the case of Io, there is ample evidence of more active interactions. Besides the direct manifestations of activity, the absorption cross-section depends upon the satellite gross characteristics.

Io and Its Torus

The energetic ion population above 10 keV/nuc is known to dominate the plasma stress throughout the regions of the magnetosphere so far studied, except for the central regions of the Io torus itself. Measurements of energetic ion stresses parallel and perpendicular to the magnetic field are essential to understanding the overall stress balance and configuration of the magnetosphere. Furthermore, energetic ion stresses and their gradients are important for magnetohydrodynamic instabilities such as the interchange and ballooning instabilities. Centrifugally-driven interchanges in particular are believed to be the dominant mechanism for transporting sulfur and oxygen ions out of the Io torus.

A low periapsis orbit would permit exploration of the Io L-shells at lower altitudes. It would even be possible to stay on the same L-shell for an extended length of time and perform detailed energy and angular distributions, including their altitude dependences. Either orbit could be used to investigate azimuthal dependences as they relate to distance from Io, and to the tilted and eccentric planetary magnetic field.

Encounters with the Io flux tube itself, and with its Alfven wings, will be possible and should be designed into the mission. This would tell a lot about particle acceleration, decametric emissions, field-aligned currents, double layers, etc. Pioneer 11 had a near encounter with the Io flux tube at a high southern latitude, with results which were quite different from the Voyager I encounter very near Io itself. Repeated encounters at all altitudes would be very desirable for determing the linkage between Io and the planetary atmosphere.

Inner Zone

With the low periapsis orbit, the motion of the argument of perigee causes the orbit to intersect the equator at all altitudes from perijove to apojove, and also to cross the L<6 lines of force at progressively higher latitudes. It would not take an unreasonable spacecraft lifetime to obtain a complete radial and latitude mapping of particle fluxes and behavior. This is the region of the highest energy, locally-accelerated particles in the solar system, and it is a unique one for trapped radiation studies, because here synchrotron losses from the energetic electrons enter into the energy balance and particle transport equations. Investigating this region has astrophysical applications, because of radio galaxies and supernova remnants that emit synchrotron radiation. It would be a concrete backbone to many an ethereal theory if we understood in detail the only case which is accessible to in situ measurements. All of the mechanisms discussed in this section that pertain to particle acceleration, losses, transport, collective behavior, and electromagnetic emissions can conceivably be found in other worlds.

A NOTE ON JUPITER'S "GOSSAMER" RING

D. A. Mendis, J. R. Hill and W. Fillius

Center for Astrophysics and Space Science

University of California, San Diego

La Jolla, CA 92093

and

T. G. Northrop

Laboratory for High Energy Astrophysics

NASA Goddard Space Flight Center

Greenbelt, MD 20771

May 1985

ABSTRACT

The newly discovered "gossamer" ring of Jupiter, composed largely of micron-sized grains, exhibits a significant peak very near the synchronous radius. The discoverers believe that this peak may be associated with an unobserved source consisting of large bodies that straddle the synchronous orbit. Here we offer an alternative evolutionary mechanism, namely the "gyrophase" drift towards the synchronous orbit, of fine grains, which necessarily are electrostatically charged within the Jovian magnetosphere.

From a re-examination of a Voyager 2 photograph in forward scattered light, Showalter et al[1,2] report the discovery of a very tenuous ring of Jupiter, largely composed of micron-sized grains, extending outward from the brighter thin inner ring to a radial distance of about 210,000 km. The existence of this ring, which they have named the "gossamer" ring, was also hinted at in the earlier Pioneer 10 data[3] as these authors state.

While its brightness in forward-scattered light seems to decrease roughly linearly with radius (with a mean value of only about 5% that of the inner ring), the authors note the significant (at the 4σ level) brightening at a radial distance of 160,000±2000 km (see their Figure 2), very close to the synchronous orbit (which is about 160,200 km). This short note addresses the possible origin of this peak near the synchronous orbit.

Showalter et al[2] believe that plasma drag is the dominant evolutionary process which transports the Jovian ring material[4] . Since the plasma drag moves material away from the location of the synchronous orbit in both directions (with a time scale they estimate to be $\sim 10^{3\pm1}$ yr for micron-sized grains), they suggest a population of larger bodies ("mooms") straddlying the synchronous orbit as the source for these small grains that form the peak. They also point out that the gossamer ring might be brighter at the synchronous distance because it has less vertical extent there, which, given the shallow viewing angle of Voyager 2, would lead to a brightness enhancement.

Here we propose an alternative origin. While one cannot exclude either possibility, there is no physical reason for natural satellites to be at the synchronous orbit except by pure chance. There is, however, an electodynamic process that causes micron-sized grains to rapidly migrate towards the synchronous orbit of Jupiter from both sides if they carry a negative electrical

charge, as has been pointed out earlier[5-7]. This is the radial "gyro-phase" drift of negatively charged grains in the Jovian magnetosphere. Hill and Mendis[5,6] showed that fragile interplanetary micrometeoroids, on penetrating the Jovian plasmapause (30-35 R_J), become rapidly charged to high electrostatic potentials ($\sim$ -100 V). These grains, or their electrostatic disruption products, have their initial, purely gravitational orbits modified by the electromagnetic forces within the magnetosphere. The grain surface potential is affected by the relative speed between the grain and the plasma, and this speed varies at the gyrofrequency. The small but finite capacitance of the grain leads to finite times of charging and discharging, and introduces into the potential a lag with respect to the gyrophase. Because of this lag, the maximum and minimum potentials are not exactly at perijove and apojove, but are displaced slightly from them. The consequence is that these grains gradually drift towards the synchronous orbit, where the velocity of a particle through the plasma is almost constant, and the radial speed slows greatly.

This radial drift, dubbed the "gyro-phase' drift, has been subsequently studied analytically in the adiabatic approximation by Northrop and Hill (1983). All guiding center drifts ($\underset{\sim}{E} \times \underset{\sim}{B}$, grad B, curvature B, etc.) occur because the curvature of the charged particle's trajectory oscillates at the gryo-frequency. All the above drifts are azimuthal when $\underset{\sim}{E}$ is radial and $\underset{\sim}{B}$ is axisymmetric. But for charged grains the drift is not exactly azimuthal due to the gyrophase lag associated with their finite capacitance, discussed above. Also, since the main modulator of the grain potential is the ion current which is largely determined by the relative speed between the grain and the plasma, a negatively charged grain is least negatively charged when, in its gyrophase, it is approximately farthest from the synchronous distance,

this being true whether the grain is outside or inside the synchronous orbit. As a result this radial drift of negatively charged grains is always towards the synchronous radius in the Jovian magnetosphere. Northrop and Hill[7] also showed that this drift continues as long as the magnetic moment of the grain is non-zero. However, the gyro-radius and therefore the magnetic moment of the grain decreases towards zero as it drifts towards the synchronous radius. The magnetic moment may vanish and the orbit may become circular around Jupiter somewhat before the grain reaches the synchronous distance. On the other hand, the orbit may happen to circularize (magnetic moment may vanish) just at synchronous radius, or the particle's guiding center may even arrive at synchronous radius with non-zero magnetic moment. What happens depends on the location and velocity with which the particle is launched. In any case, one expects a maximum in the concentration of fine dust at the synchronous orbit regardless of the sources and their locations. We agree with Showalter et al[2] that grains can remain in stable orbits at the synchronous distance, whether they are charged or not, since the plasma drag there is zero on all grains. However, only grains that are electrically charged can be transported <u>toward</u> the synchronous distance, wherever they happen to originate. Thus our mechanism makes no particular demands on the location of the source or sources and in particular does not require them to be at synchronous radius.

This process proceeds with a timescale of only a few years for micron-sized grains[6,7] and is thus much faster than any disruptive process (e.g., sputtering by energetic particles) for the grains or the systematic drift (away from synchronous orbit) caused by plasma drag. Even if the gyro-phase drift proceeds 1-2 orders of magnitude slower, due to the possible overestimation of the highly uncertain plasma temperature and density near the

ring plane, this process is still the fastest evolutionary one. In fact, Hill and Mendis[6] earlier suggested just this process for the formation of the inner ring. However, the fact that it was substantially inside the synchronous orbit, as well as its proximity to the newly discovered small satellites Metis and Adrastea, made this an unlikely explanation. We too believe that these satellites represent a secondary source for the inner ring, on being bombarded by incoming micrometeoroids.

Using the optical depth of 10^{-7} and vertical extent of 2000 km (which is a factor of 2 smaller than the upper limit given by Showalter et al[2], we find that the intergrain separation ($\sim$5m) is significantly larger than the Debye length ($\sim$ 1m) for reasonable values of the rather uncertain plasma parameters near the ring. Consequently, collective effects that tend to decrease the grain charge[8,9] do not complicate the "isolated particle" approach used by these authors[5-7].

In their study of the ~~adiabatic~~ motion of charged dust grains, Northrop and Hill[7] also obtained an "energy-like" exact constant of motion which is valid even though the grain charge varies arbitrarily with time. The use of this constant enables us to calculate directly the "circularization radius" of a grain, given its initial position, velocity and charge-to-mass ratio. For example, a grain with large charge-to-mass ratio launched at the Kepler velocity from Thebe (3.11 R_J) circularizes at ~~2.62~~ $\sqrt{}$ or K R_J, while a 0.5μm grain charged to -10 V circularizes at ~~2.48~~ 2.757 R_J. On the other hand, the initial azimuthal velocity needed for the circularization radius to be the synchronous radius is independent of charge to mass, ~~as long as the adiabatic requirements are satisfi~~ed. We have ~~used this method to~~ calculate the initial projection velocities of grains (assumed ejected in the azimuthal direction) needed to just circularize at synchronous radius. For instance, a grain emitted from

Thebe (3.11 R_J) circularizes at synchronous (2.24 R_J) if it is ejected at velocities, with respect to the moon, of either 32.2 km s^{-1} (direct) or 1.9 km s^{-1} (retrograde). Grains that are emitted with larger speeds (in either direction) will also reach the synchronous radius, but with finite magnetic moment, so that they would not be circularized there. Nevertheless, their radial motion would be greatly reduced. The corresponding velocities for grains ejected from Amalthea (2.54 R_J) are, respectively, 11.5 km s^{-1} (direct) and 0.8 km s^{-1} (retrograde), while those for grains ejected from "mooms" at the outer edge (1.81 R_J) and the inner edge (1.72 R_J) of the bright ring, inside the synchronous orbit, are, respectively, 1.5 km s^{-1} (direct) 12.5 km s^{-1} (retrograde); 1.9 km s^{-1} (direct) and 9.1 km s^{-1} (retrograde). While these larger speeds of projection required from the moons (direct outside synchronous and retrograde inside) appear to be excessive, considering the large yields expected at hyper-velocity impacts[4], the smaller speeds of 1-2 km s^{-1} (retrograde outside synchronous and direct inside) are reasonable values for the ejecta resulting from the bombardment of these small moons by incoming interplanetary micrometeoroids.

A more refined calculation should take into account the finite inclination of the magnetic axis of the planet to the spin axis, which would make the grain also perform an oscillation about a plane intermediate to the magnetic and geographical equators[7]. Radial gradients in the plasma temperature and density (which were ignored in the aforementioned calculation) could also change the picture somewhat, and in particular change the evolutionary timescale, because under certain circumstances they could conspire to cause a secular increase in the magnetic moment of the charged grain [10]. Unfortunately, the plasma parameters near the Jovian ring plane are too uncertain at the present time to merit the study of such second-order effects.

We acknowledge these uncertainties and recognize the need for more detailed calculations in the future, taking these processes, as well as the effects of plasma drag and radiation pressure, into consideration. The main purpose of this short note, however, is to emphasize the existence of an evolutionary process (namely the gyro-phase drift) which can cause radial transport of fine dust grains (which are necessarily electrically charged within the Jovian plasmasphere) towards the synchronous distance from both sides. We believe this to be the process responsible for the peak in the "gossamer" ring near the synchronous radius. Conversely, we find the peak at the synchronous radius to be persuasive evidence that the grains are electrically charged to some negative potential with respect to the ambient plasma.

Acknowledgements

REFERENCES

1. Showalter, M. R., J. A. Burns, and J. N. Cuzzi, Jupiter gossamer ring, abstract in Bull. Amer. Astr. Soc., 16, 674-675, 1984.

2. Showalter, M. R., J. A. Burns, J. N. Cuzzi, and J. B. Pollack, The discovery of a tenuous Jovian ring, submitted to Nature, 1985.

3. Humes, D. H., J. M. Alvarez, R. L. O'Neal, and W. H. Kinard, The interplanetary and near-Jupiter meteoroid environment, J. Geophys. Res., 79, 3677-3684, 1974.

4. Burns, J. A., M. R. Showalter, and G. E. Morfill, The ethereal rings of Jupiter and Saturn, in Planetary Rings (R. Greenberg and A. Brahic, eds.), University of Arizona Press, Tucson, Arizona, 1984, pp. 200-272.

5. Hill, J. R., and D. A. Mendis, Charged dust in outer planetary magnetospheres. I. Physical and dynamical processes, Moon and Planets, 21, 3-15, 1979.

6. Hill, J. R., and D. A. Mendis, Charged dust in outer planetary magnetospheres. II. Trajectories and spatial distributions, Moon and Planets, 23, 53-71, 1980.

7. Northrop, T. G., and J. R. Hill, The adiabatic motion of charged dust grains in rotating magnetospheres, J. Geophys. Res., 88, 1-11, 1983.

8. Goertz, C. K., and W-H. Ip, Limitation of electrostatic charging of dust particles in a plasma, Geophys. Res. Letts., 11, 349-352, 1984.

9. Whipple, E. C., T. G. Northrop, and D. A. Mendis, The electrostatics of a dusty plasma, J. Geophys. Res., in press, 1985.

10. Mendis, D. A., Adv. Space Res., 4, 111-120, 1984.

N86-13281

ELECTRONS AND COSMIC RAY PRODUCED PROTONS IN SATURN'S INNER MAGNETOSPHERE

T. G. Northrop
NASA/Goddard Space Flight Center
Greenbelt, MD 20771

and

Walker Fillius
Center for Astrophysics and Space Sciences
University of California, San Diego
La Jolla, CA 92093

ABSTRACT

The University of California Cerenkov detector on Pioneer 11
previously observed Crand protons above 600 MeV in Saturn's inner
magnetosphere, mixed with a poorly understood background of energetic
electrons [Fillius and McIlwain, 1980]. Here we separate the electron from
the proton counts and establish the first-order angular distributions for each
species. To do this we use the theoretical relationships among the harmonic
coefficients of the count rate as a function of spacecraft roll angle derived
by Northrop [1985]. The majority of the counts were electrons with energy
above several MeV; ie, with drift periods shorter than the satellite orbital
resonance. The electrons have isotropic pitch angle distributions, and the
protons pancake over most of the region between Mimas and the rings, although
there is a small region of dumbbell proton distributions in the vicinity of
Janus and Epimetheus.

INTRODUCTION
.

There was an internal inconsistency in the data taken at Saturn by the University of California, San Diego Cerenkov detector on Pioneer 11. East-west anisotropies observed between the outer edge of the A ring at 2.28 R_s and Mimas at 3.09 R_s apparently belonged to protons below the known response range of the detector. In the original analysis, Fillius and McIlwain deduced the gyroradius by using Liouville's theorem to interpret the radial displacement necessary to align the measured eastbound and westbound fluxes. The discrepancy was tentatively attributed to the presence of background electrons, but there was no method to quantify the contribution of these particles. Here we use the theory developed by Northrop in the accompanying paper to decompose the Cerenkov detector output into two components, belonging to high-rigidity protons and low-rigidity electrons. With this analytical tool we can give estimates of the proton and electron fluxes and, to a limited extent, their angular distributions. The results revise the high end of the energy spectrum of trapped protons created by the Crand mechanism, and reveal the existence of energetic electrons whose spatial distribution is unlike that of the lower energy electrons.

To show the instrumental dilemma we first present an essential description of the detector and relevant calibrations. From the proton response we conclude that the east-west anisotropy was produced by protons of energy ~600 MeV. Because the energy spectrum of the electron background is not well determined, we also include a description of the electron response in order to evaluate two different possibilities. Then we review the observations briefly, and show how we apply Northrop's method to separate the particle species.

PROTON RESPONSE OF THE CERENKOV DETECTOR

The UCSD Cerenkov detector on Pioneers 10 and 11 has a radiator of 60/40 methanol/water with index of refraction of 4/3. The liquid is held in a 14 X 75 mm bottle of ultra-pure fused silica the front end of which is occupied by an expansion bellows for thermal compensation between the liquid and the bottle. The radiator is viewed at one end by a photomultiplier tube and associated electronics which count pulses above three discrimination levels (labeled C1, C2, and C3). No coincidence detectors are used because the high fluxes of Jupiter's radiation belts would have paralyzed the necessary circuitry. Instead, directionality is achieved by internal reflection of light emitted toward the photomultiplier, and absorption of light traveling in the other direction on the bellows and blackened inner walls of the radiator housing. The discrimination levels are set so that the lowest channel (C1) can be triggered by a particle whose pathlength in the radiator is not much more than a diameter, but the highest channel (C3) requires a pathlength comparable to the length of the radiator. Thus the channels have different angular responses, from C1 with significant side sensitivity, to C3 with a pencil lobe in the forward direction only.

The angular response of the Cerenkov detector was demonstrated with an identical unit in the proton beam of the NASA Space Radiation Effects Laboratory (SREL) synchrocyclotron. The detector was rotated and its effective cross-sectional area was normalized to that of a monitor detector. Figure 1 shows the effective area vs angle from the detector look axis for channel C3.

When operating in a space radiation environment, the detector is irradiated simultaneously from all angles, and here the most useful calibration is the integral of the effective area over solid angle, called the geometric factor,

$$G(E) = \int A_{eff}(E) \, d\Omega$$

Figure 2 shows the geometric factor as a function of energy for several discrimination levels. Because the principal effect of varying the discrimination level is to vary the pathlength needed to yield enough light, the principal difference between channels is in the width of their angular

responses, and so, in the magnitude of their geometric factors. The energy threshold is a second-order effect because all protons near the threshold easily have enough range to penetrate the entire detector and thus to produce the same pathlength. The channel to channel differences in energy threshold are primarily due to the fact that the lower channels are able to respond to Cerenkov light produced in the bottle walls and faceplate. For the index of fused silica, 3/2, the critical proton energy is 320 MeV. This accounts for the incipient response evident in channels C1 and C2 in Figure 2, but it is not a major factor because, with only a small amount of fused silica, it requires exceptionally favorable particle trajectories.

The peak energy of the SREL synchrocyclotron was not high enough to complete the response curve of the detector. To calibrate the asymptotic high-energy response, we used cosmic ray muon counting rates observed in our laboratory, corrected for the effect of the muon angular distribution over the angular response of the detector. These asymptotic geometric factors are plotted on the right-hand axis of Figure 2.

The channels labeled C1, C2, and C3 in Figure 2 were matched to the prelaunch discrimination levels of the Pioneer 10 and 11 Cerenkov detectors. Both of these detectors underwent subsequent gain changes because of the high level radiation during the Jovian encounter. The effect on the Pioneer 11 Cerenkov detector was to increase the photomultiplier tube gain, which is equivalent to lowering the discrimination levels. The channel in Figure 2 marked C3′ is interpolated from C2 and C3 to the level of Pioneer 11 channel C3 during the Saturn encounter. In this section and in the following one on the electron response of the Cerenkov Detector, we use the labels C1, C2, and C3, without a prime, to refer to the discriminators at their calibrated prelaunch levels, and we add a prime (e.g.: C3′) to distinguish the levels realized at encounter. In our discussions of flight data, we use actual readings -- at the discrimination levels as they occurred. We drop the prime then, as the distinction is superfluous, and when we discuss our observations and conclusions, an unprimed label refers to the changed discriminator at the time off encounter.

The small bump at ˜100 MeV is caused by scintillation of protons that

stop in the optical materials. As mentioned by Fillius and McIlwain [1980], this represents an omnidirectional geometric factor of $< .002$ cm^2 for protons between 65 and 140 MeV. By comparison, the UCSD solid state detector on Pioneer 11 has a geometric factor of $.012$ cm^2 over a larger energy window between 80 and several hundred MeV. Then by comparing the counting rates of these two sensors, we can conclude that no more than about 12%, of the C3 response is caused by proton scintillation.

ELECTRON RESPONSE OF THE CERENKOV DETECTOR

The Cerenkov detector is also sensitive to electrons. (Its primary mission was to measure the intensities of high energy electrons in the Jovian environment.) Figures 3 and 4 show the measured electron response. For electrons, unlike protons, penetration range is an important factor in understanding the detector response. The first important threshold is the energy ($\sim$0.7 MeV) required for an electron to penetrate the detector housing. Since electrons are relativistic at this energy, the next criterion is the length of their track in the radiator, which determines their Cerenkov light output. As with protons, the particle trajectory must point toward the back end of the radiator in order to direct the Cerenkov beam to the cathode. The electrons' propensity to undergo high-angle scattering collisions has two effects. One is that the range tends to be overstated by tables which list "end-point values," or the range of a scatterfree particle, and the other is that the angular responses tend to be smeared.

Figure 3 demonstrates the net result for channel C3. Full response occurs at high energy where the particles' range exceeds the length of the radiator and the relativistic mass gain reduces their tendency to scatter. The biteout along the axis has two causes. One is that the asymptotic Cerenkov emission angle equals the critical reflection angle, so that light starts to be lost. The other is that there is more passive shielding at the front end of the housing than on the sides. As the electron energy decreases, the dominant response occurs on the side, where the radiator has a larger cross-sectional area, but smaller depth. Ultimately, as the electron energy decreases, the pulse height falls below the discrimination level. Then the

electrons can only trigger the detector if several arrive simultaneously so
that their pulses add in height. In this mode the response is peaked to the
side where the cross-sectional area is largest. Channels C1 and C2 operated
in this mode during the most intense segment of the Saturn flyby.

Figure 4 shows the geometric factor for single-particle events,
plotted as a function of energy. This represents the detector's response to a
delta function energy spectrum. It is convenient to represent this profile as
a step function, so that we can quote the flux above some threshold. We
previously used Van Allen's "bow-tie method" to obtain such a representation
applicable to the Jovian radiation environment [Fillius and McIlwain, 1974].
However, at Saturn, the electrons causing the pileup on channels C1 and C2
have an extremely soft spectrum, outside the range of anything encountered
previously. As the bowtie method showed, the same threshold value is not
applicable for all spectra. Therefore, we have listed in Table I threshold
energies applicable to a range of power law energy spectra, of the form,

$$dN/dE = - K E^{-n}$$

This table should help in interpreting the detector's response to very soft
electron spectra.

Table I

Threshold energies for channel C3
effective for different power law energy spectra
with a geometric factor of 0.5 cm^2-sr

n	E_{th}
1	14
2.5	14
4	12
6.3	10
10	8.5

OBSERVATIONS

The channel C3 counting rate reached a maximum in the vicinity of 2.7 R_s ($1R_s = 60,000$ km) and fell off to zero and near-zero values at the outer edge of the A ring (2.28 R_s) and the orbit of Mimas (3.09 R_s). The east-west anisotropies that we are investigating are associated with the gradients on either side of the peak. Using a least-squares fitting procedure, Fillius and McIlwain [1980] represented the angular distribution of the counting rate by a truncated Fourier expansion of the form $C = C_0 + C_1 \sin(X) + C_2 \cos(2X) + C_3 \sin(3X) + \ldots$, X being the angle between the look direction of the detector and the magnetic field, which happened to lie in the scan plane. Terms were chosen for symmetry and economy: omitted terms would violate mirror symmetry, and coefficients above $3X$ were so heavily convolved by the width of the sampling interval that they could not be evaluated with our limited amount of data. In this representation the coefficient C_0 is the spin-averaged count rate; the omnidirectional count rate is $C_0 - C_2/3 - C_4/15$. The coefficient C_2 reflects whether the peak of the distribution is perpendicular to the magnetic field ($C_2 < 0$) or parallel to it ($C_2 > 0$). The former case is called a pancake distribution and the latter, a dumbbell. The east-west anisotropy appears in the odd harmonics C_1 and C_3.

The coefficients derived from the data are shown in Figures 5 and 6 for the inbound and outbound radial cuts of Pioneer 11. The smooth curves were merely drawn by eye through the points. Note that outbound C_0 and C_2 have quite similar shapes, and inbound they are similar, too, although the peaks are not quite coincident. In Figure 6 there was a data gap between 2.38 R_s and 2.49 R_s. This has been filled in by interpolation so as to be able to carry out integrals over the entire range. Results inside 2.49 R_s outbound are therefore not to be trusted and will not be given in later figures.

SEPARATION OF PROTON FROM ELECTRON COUNTS

The observed coefficients are assumed to be sums of proton and electron components. Thus $C_0 = C_{0p} + C_{0e}$, and similarly for the higher

harmonic coefficients. We assume that there is no pile-up in this channel and no counts lost to dead time. In the preceding paper Northrop [1985] derived relationships among the harmonic coefficients of the proton and electron count rate as a function of roll angle. Because the electrons have very small gyroradius, their odd harmonics vanish, and the odd harmonics observed are attributed entirely to protons. The even proton coefficients are given by equations (14) and (15) of that paper:

$$C_{2p}(r) = C_{4p}(r) + 2r^6 \left[\frac{r_1 3}{\rho_p(r_1)\cos\theta} \int_{r_1}^{r} dy \frac{C_{3p}(y)}{y^9} + 9 \int_{r_1}^{r} dy \frac{C_{4p}(y)}{y^7} \right] \quad (1)$$

$$C_{0p}(r) = \frac{C_{4p}(r)}{2} + \frac{r_1 3}{\rho_p(r_1)\cos\theta} \left[\int_{r_1}^{r} dy \frac{C_{1p}(y) - C_{3p}(y)}{y^3} + 2r^6 \int_{r_1}^{r} dy \frac{C_{3p}(y)}{y^9} \right.$$

$$\left. + 6 \int_{r_1}^{r} dy \frac{C_{4p}(y)}{y} \left(\frac{3r^6}{y^6} - 1 \right) \right] \quad (2)$$

where r_1 is some point at which the count rate vanishes (say the outer edge of the A ring), and $\rho_p(r_1)$ is the proton gyroradius at r_1. Based on the detector calibrations (See Figures 1 and 2), we used a proton energy of 600 MeV to calculate the gyroradius. The integrals were performed by Simpson's rule upon the smooth curves. This is a bit subjective, but, unlike differentiation, integration tends to even out random errors in the input. Once C_{0p} and C_{2p} are known, C_{0e} and C_{2e} are given by $C_{0e} = C_0 - C_{0p}$ and $C_{2e} = C_2 - C_{2p}$.

Coefficient C_4 is absent from Figures 5 and 6 because there were not enough data to determine it directly as a function of r. We have assumed that C_4 has the same shape as the other even coefficients and determined the ratio $b = C_4/C_0$ from the integral conditions (16) and (17) of the preceding paper. The conditions use the fact that the fluxes vanish at both boundaries of the region of interest. This method gives two values for b, one from each equation, and unless they agree, there is a dilemma. We find that inbound b = 0.0915 and 0.0881 from (16) and (17) respectively. This minor discrepancy is handled by using 0.0915 in (1) and 0.0881 in (2) -- that is, by using b in the equation from which it was determined. One may prove that the value of (1) or (2) is independent of whether one integrates from r_2 inward, or from r_1 outward to the r of interest, provided that the b used in the equation was determined from it. Outbound the two values of b determined from (1) and (2) disagree: (1) gives b = 0.00467 and (2) gives b = -0.0130. In this case we have again used the b in the equation from which it came. The disagreement may be a consequence of the data gap.

Figures 7 and 8 give the omnidirectional count rates for protons and electrons, and Figures 9 and 10 are the pitch angle distributions to lowest order in gyroradius. (The f_0 from equation 3 of the preceding paper.) We immediately see that the proton count rate was only 20% of the electron rate. The proton angular distribution is found to be pancake (except in the vicinity of Janus and Epimetheus where they are dumbbell) and the electrons are isotropic. Both angular distributions agree with what one expects from cosmic rays as the source, striking ring material in the case of the protons, or the moons Mimas, Janus, Epimetheus, and rings for electrons [Blake et al., 1983]. However according to Blake [1985] the flux of electrons produced by cosmic rays, although approximately isotropic, would be much smaller than in Figures 7 and 8. Another source, such as diffusion past Mimas from outside, is required, and it would have to be verifed that such a source should give an isotropic flux. That cosmic rays produce protons by the Crand process in the inner region of Saturn's magnetosphere was first suggested by Fillius et al. [1980] and also by Cooper and Simpson [1980], Van Allen et al. [1980], and McDonald et al. [1980]. Van Allen found that his protons $\lesssim$ 80 MeV) were pancake in this inner magnetosphere. Other papers have subsequently studied the pitch angle distribution. If that distribution is modeled by $\sin^n(\delta)$, a

value of n=6 at 3.5 R_s has been reported by Vogt et al, [1982]. Krimigis and Armstrong [1982] find n=5. Schardt and McDonald [1983] find that for 48-160 MeV protons n increases from ~1 at 2.7 R_s to nearly 5 at 2.85 R_s.

DISCUSSION: INBOUND DATA

The peak of the proton omnidirectional flux occurs at larger radial distance than the electron peak. (There is no theoretical reason for the peaks to coincide.) That there should be a proton peak is to be expected: Crand is a distributed source of protons, and the A ring, Janus-Epimetheus, and Mimas are sinks for the protons, which diffuse both ways from the interior of the region under study. Cooper [1983] has solved the problem of the Crand source plus diffusion to absorbing edges and fit the University of Chicago data from Pioneer 11. From Figure 7 the peak for 600 MeV protons is at 2.72 R_s, and there is a minimum at 2.52 R_s at the radius of Janus and Epimetheus, leaving a secondary peak at 2.4 R_s that is about 1/3 the height of the main peak. The position of the main peak and the factor of 1/3 both coincide with the profiles determined by Van Allen et al [1980] and Fillius and McIlwain [1980] for energies > 80 MeV. There is no discernible absorption by the G-ring at these >600 MeV energies, in contrast to lower energies where all experiments see an effect (See, for example, Van Allen [1983]).

The proton angular distributions (Figure 9) are pancake outside Janus-Epimetheus and are dumbbell in the minimum. The upswing at low count rates of these angular distributions is probably not real, nor are negative values. There is much scatter in these deduced distributions, which is not surprising considering the long train of analysis. The proton distribution goes approximately as $\sin^5(\delta)$ at the peak (2.72 R_s), but we cannot determine any trend at larger radii, although theory predicts more isotropy [Cooper, 1983].

In contrast to protons, there is no significant volume source of electrons of the proper energy within the region. Two different sources of electrons are possible. High energy electrons are produced by cosmic rays at the rings and at Mimas, [Blake et al., 1983] and diffuse toward the center of

the region from these sources at the two edges. The energy of these electrons is tens of MeV, and so they are well up on the plateau of the detector response (See Figure 4). This source is too weak, as mentioned earlier, and there should not be a peak at 2.62 R_s, given the location of the sources.

Secondly, electrons from other sources, outside Mimas, may be diffusing inward. The spectrum of these electrons is soft, because the preferred energy for electrons to escape absorption by Mimas is just 1 MeV, and by 7 MeV the relative drift time has fallen from infinity to <5 hours. As compiled by Chenette and Stone [1983], the electron spectrum at Mimas falls by 4 orders of magnitude between 5 MeV and 11 MeV. Magnetic-moment-conserving diffusion of relativistic electrons from Mimas to the electron peak at 2.62 R_s increases the energy of electrons with 90° pitch angle by a factor of 1.3. With the steeply falling energy spectrum, this energization would increase the number of electrons above the energy threshold by a factor of 18. The count rates at Mimas were small, at most a few per second, so it seems that a peak of 315 per second is too large to be accounted for completely in this way. If the spectrum at Mimas were actually steeper than the best estimate by Chenete and Stone, then radial diffusion could fit the observations. The spectrum would have to fall 7 orders of magnitude rather than 4, and this conceivably could be the case [Chenette, 1985]. This, plus some absorbtion by Janus and Epimetheus might explain the electron curve in Figures 7 and 8.

An alternative would be to invoke episodes of strong diffusion, followed by quiescent periods during which wipeout continues. This has been analyzed by McKibben and Simpson [1980] and qualitatively can explain how there might occur an increasing inward phase space density at constant magnetic moment even in the absence of an interior particle source.

OUTBOUND DATA

The electron peak is comparable in height with the inbound electron peak but is at a larger radius than inbound. As inbound, the electron angular distributions are quite isotropic. The radial profile of the electrons is different from that observed at lower energies, in that it is peaked, and

vanishes at the orbits of Mimas and at the F ring. At lower energies (~1 MeV) the electrons do not exhibit clear channels at the orbits of these moons, which is consistent with their resonant energy to avoid sweeping.

The peak in proton flux in Figure 8 is at the same radius (2.72 R_s) as inbound and is at just about the same height. As at lower energies (e.g., above 80 MeV [Van Allen et. al, 1980; Fillius and McIlwain, 1980]) there appears to be azimuthal symmetry about Saturn. Although we have no data inside 2.49 R_s, there is no evidence in Figure 8 of an incipient upturn of the curve inward of 2.5 R_s. Van Allen does see wings of a secondary peak outbound that he estimates would have been lower than inbound by a factor of 2 to 3. The inbound-outbound asymmetry of Crand protons at the radius of Janus and Epimetheus may in some way be produced by these moons, but not by a simple wipeout mechanism. The Crand source is so weak that the protons from it must have lifetimes of years to produce the observed fluxes. Such a long lifetime implies too slow radial diffusion for these moons to produce azimuthal asymmetry. The protons would not diffuse rapidly enough to fill in behind the moons and thereby produce visible asymmetry.

The proton angular distributions are pancake except near Janus and Epimetheus where they are dumbbell -- just as was the case inbound. The pancake distributions are less well organized than inbound. We do not know whether this is real or merely represents the noise in the analysis, which is not completely satisfying because of the determination of C4 and the data gap. Nevertheless, the results of the analysis agree remarkably well with the inbound pass, and with observations at lower energies (>80 MeV).

CONCLUSIONS

1. We have employed the method developed by Northrop in the accompanying paper [1985], for deducing the omnidirectional intensity and first-order angular distributions of high-rigidity particles in the presence of a background of low-rigidity particles. The method is applied by performing appropriate integrals over the observed angular distributions, and

can be thought of as an integration of the radial gradient deduced from the east-west anisotropy of the high-rigidity particles.

2. We have evaluated the number of 600 MeV protons necessary to produce the east-west anisotropy observed by the UCSD Cerenkov detector on Pioneer 11 between 2.3 and 3.1 R_s. This is a significant downward revision of the estimate made by Fillius and McIlwain [1980]`, but nevertheless still consistent with other data at lower energies. Crand is the most likely source for these particles, as concluded by Fillius and McIlwain [1980].

3. There exists a high energy component of the electron spectrum which has a spatial profile with low values at Mimas and Janus-Epimetheus and a maximum in between. This profile indicates that sweeping takes place at these moons, which is to be expected for electrons of several MeV or more. The source and spectrum of these electrons remains uncertain.

4. We have determined the pitch angle distributions of these particles to first order in gyroradius. The electrons are almost isotropic, but the protons exhibit a combination of pancakes and dumbbells, with the latter near Janus and Epimetheus.

REFERENCES

Blake, J. B., H. H. Hilton, and S. H. Margolis, "On the Injection of Cosmic Ray Secondaries Into the Inner Saturnian Magnetosphere: 1. Protons From the Crand Process," J. Geophys. Res., 88, 803, 1983.

Blake, J. B., Private communication 1985.

Chenette, D. L., and E. C. Stone, "The Mimas Ghost Revisited: An Analysis of the Electron Flux and Electron Microsignatures Observed in the Vicinity of Mimas at Saturn," J. Geophys. Res., 88, 8755, 1983.

Chenette, D. L., Private communication, 1985.

Cooper, J. F., and J. A. Simpson, "Sources of High-Energy Protons in Saturn's Magnetosphere," J. Geophys. Res., 85, 5793, 1980.

Cooper, J. F., "Nuclear Cascades in Saturn's Rings: Cosmic Ray Albedo Neutron Decay and Origins of Trapped Protons in the Inner Magnetosphere," J. Geophys. Res., 88, 3945, 1983.

Fillius, W., W.-H. Ip, and C. E. McIlwain, "Trapped Radiation Belts of Saturn: First Look," Science, 207, 425, 1980.

Fillius, W., and C. E. McIlwain, "Very Energetic Protons in Saturn's Radiation Belt," J. Geophys. Res., 85, 5803, 1980.

Krimigis, S. M., and T. P. Armstrong, "Two Component Proton Spectra in the Inner Saturnian Magnetosphere," Geophys. Res. Lett., 9, 1143, 1982.

McDonald, F. B., A. W. Schardt, and J. H. Trainor, "If You've Seen One Magnetosphere, You Haven't Seen Them All: Energetic Particle Observations in the Saturn Magnetosphere," J. Geophys. Res., 85, 5813, 1980.

Northrop, T. G., "Relationships Among the Harmonic Coefficients of Scan Plane Anisotropies," accompanying paper submitted to J. Geophys. Res., 1985.

Van Allen, J. A., B. A. Randall, and M. F. Thomsen, "Sources and Sinks of Energetic Electrons and Protons in Saturn's Magnetosphere," J. Geophys. Res., 85, 5679, 1980.

Vogt, R. E., D. L. Chenette, A. C. Cummings, T. L. Garrard, E. C. Stone, A. W. Schardt, J. H. Trainor, N. Lal, and F. B. McDonald, "Energetic Charged Particles in Saturn's Magnetosphere: Voyager 2 Results," Science, 215, 577, 1982.

FIGURE CAPTIONS

Figure 1

Effective Area of Cerenkov detector channel C3 as a function of angle
to the detector axis for protons of energy 66, 98, 137, 446, 497, 521, and 560
MeV. The proton energy is given at the right hand edge of each curve.
Because of experimental difficulties there is significant scatter and
statistical error, and this is illustrated for 560 MeV (circles) and 98 MeV
(crosses). These data were taken at the NASA Space Radiation Effects
Laboratory (SREL).

Figure 2

Response vs energy for several pulse height channels of the UCSD
Cerenkov detector. (For identification of the channels, see the text.) The
proton response was obtained at SREL up to its peak energy of 560 MeV, and
ground level cosmic ray muons were used to calibrate the asymptotic response
of the detector to particles with unit charge.

Figure 3

Effective area vs angle for electrons of the indicated energies..
These data were obtained on the electron linac operated by Intelcom Radtek
Corporation in San Diego.

Figure 4

Response vs energy for channels C1, C2, and C3 of the UCSD Cerenkov
detector. To represent these profiles as ideal step functions, one must allow
the value of the threshold energy to depend upon the energy spectrum of the
incident radiation. (See Table I and text.)

Figure 5

Harmonic coefficients of the count rate as a function of the
spacecraft roll angle, plotted vs. radial distance to Saturn during the
inbound pass.
(a) Even harmonics, inbound.
(b) Odd harmonics, inbound.

Figure 6

Harmonic coefficients of the count rate as a function of the
spacecraft roll angle, plotted vs. radial distance to Saturn during the
outbound pass.

(a) Even harmonics, outbound.

(b) Odd harmonics, inbound.

Figure 7

Derived omnidirectional count rates for protons and electrons on the
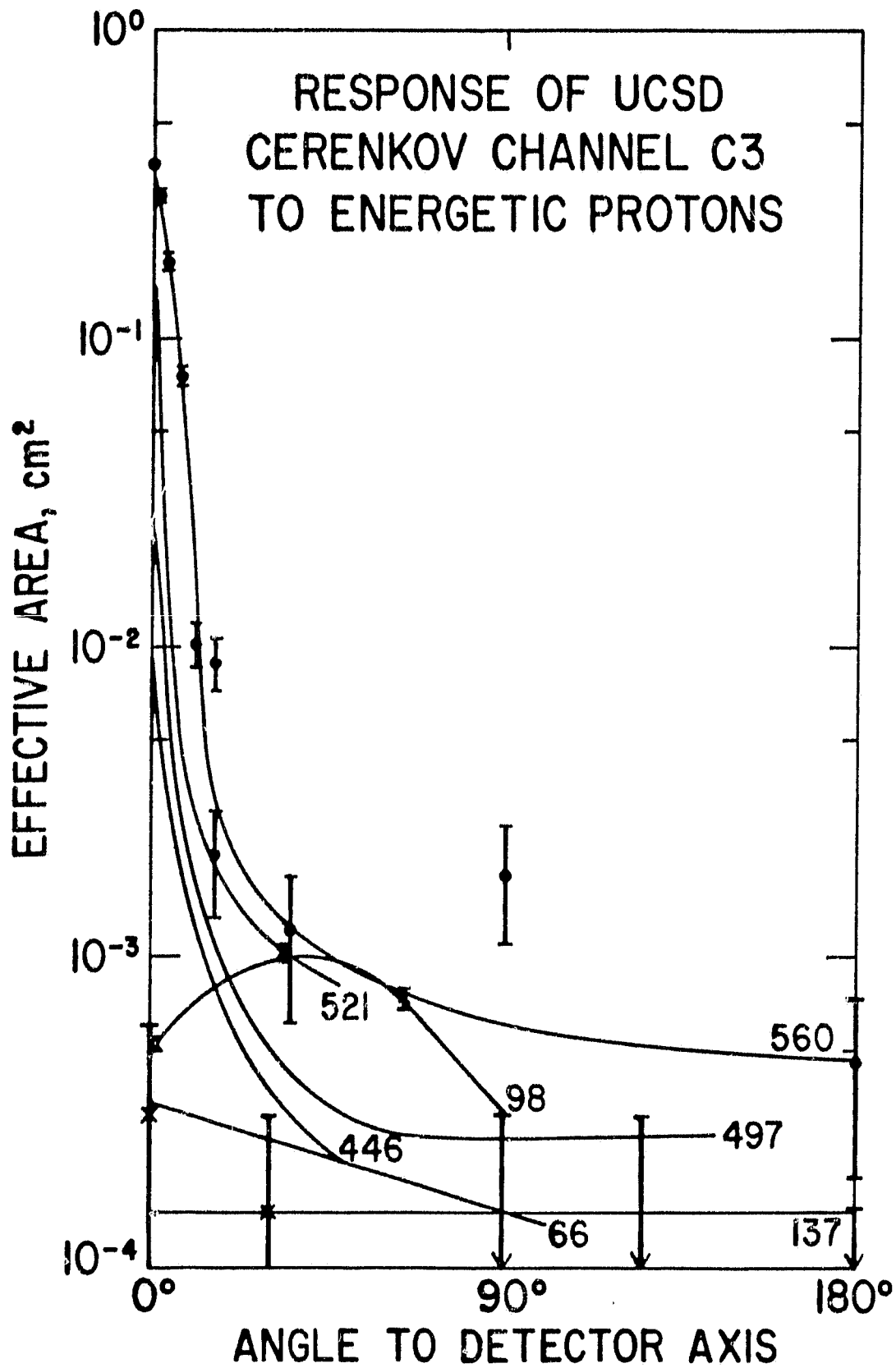inbound pass.

Figure 8

Derived omnidirectional count rates for protons and electrons on the
outbound pass.

Figure 9

Derived angular distributions for protons and electrons on the inbound
pass.

Figure 10

Derived angular distributions for protons and electrons on the
outbound pass.

RESPONSE OF UCSD
CERENKOV CHANNEL C3
TO ENERGETIC PROTONS

EFFECTIVE AREA, cm²

ANGLE TO DETECTOR AXIS

85WF-4,5-002

Fig. 1

UCSD CERENKOV DETECTOR
GEOMETRIC FACTOR

Fig. 2

19

RESPONSE OF CERENKOV
CHANNEL C3 TO
ENERGETIC ELECTRONS

69 MeV
39
31
23
16
14
10

75WF-4-005

EFFECTIVE AREA IN cm^2

1.0

0.1

0.01

0   45   90   135

ANGLE TO DETECTOR AXIS
IN DEGREES

Fig. 3

90

UCSD CERENKOV DETECTOR
DIRECTIONAL GEOMETRIC FACTORS
FOR RADIATION UNIFORM OVER
THE ACCEPTANCE LOBE

LEVEL C1

LEVEL C2

LEVEL C3

74WF-4-133

Fig. 4

Fig. 5a

Fig. 5b

23

Fig. 6a

24

Fig. 6b

Fig. 7

Fig. 8

Fig. 9

Fig. 10